Mon. Not. R. Astron. Soc. **316**, 559–568 (2000)

Gas properties of H II and starburst galaxies: relation with the stellar population

D. Raimann,[1★] T. Storchi-Bergmann,[1★] E. Bica,[1★] J. Melnick[2★] and H. Schmitt[3★]
[1]*Universidade Federal do Rio Grande do Sul, IF, CP15051, Porto Alegre 91501-970, RS, Brazil*
[2]*European Southern Observatory, Casilla 19001, Santiago 19, Chile*
[3]*Space Telescope Science Institute, 3700 San Martin Drive, Baltimore, MD21218, USA*

Accepted 2000 February 29. Received 2000 February 11; in original form 1999 October 22

ABSTRACT

We study the gas emission of galaxies with active star formation, consisting mostly of H II and starburst galaxies, as well as some Seyfert 2 galaxies, and determine chemical and physical parameters. The data consist of 19 high signal-to-noise ratio optical templates, a result of grouping 185 emission-line galaxy spectra. Underlying stellar population models (from Raimann et al.) were subtracted from the templates in order to isolate the pure emission component.

We analyse the distribution of these improved signal-to-noise ratio emission spectra in diagnostic diagrams and find that the H II templates show a smaller spread in $\log([\mathrm{O\,III}]/\mathrm{H}\beta)$ values than the individual galaxies, apparently as a result of the population subtraction and a better signal-to-noise ratio. We thus suggest the template sequence as a fiducial observational locus for H II galaxies which can be used as reference for models. The sequence of line ratios presented by the H II galaxies in the diagram $\log([\mathrm{O\,III}]\lambda5007/\mathrm{H}\beta)$ versus $\log([\mathrm{N\,II}]\lambda6584/\mathrm{H}\alpha)$ is primarily owing to the gas metallicity, of which the $\log([\mathrm{N\,II}]/\mathrm{H}\alpha)$ ratio is a direct estimator. We also study the properties of the starburst galaxies and those intermediate between H II and starburst galaxies, which are more metal rich and sit on more massive galaxies.

We discuss the present results in the frame of a recently proposed equivalent-width diagnostic diagram for emission-line galaxies (by Rola et al.) and conclude that the observed ranges in $W([\mathrm{O\,II}])/W(\mathrm{H}\beta)$ and $W(\mathrm{H}\beta)$ are mostly owing to the non-ionizing stellar population contribution. We propose that $W(\mathrm{H}\beta)$ be used as an estimator of this contribution to the continuum, and briefly discuss implications to the cosmological use of H II galaxies.

Key words: galaxies: abundances – galaxies: compact – galaxies: ISM – galaxies: nuclei – galaxies: starburst – galaxies: stellar content.

1 INTRODUCTION

The investigation of nearby star-forming galaxies plays an important role in the interpretation of the ever increasing data on distant galaxies, as the so-called Lyman-break galaxies seem to be well described by local Starburst galaxies (Meurer, Heckman & Calzetti 1999). Melnick, Terlevich & Terlevich (2000) propose that H II galaxies can be used as distance estimators over a wide range of redshifts.

H II galaxies are among the less luminous star-forming galaxies. Their emission-line spectra and relatively low gaseous metallicities (≈0.1 to 0.25 solar, e.g. Peña, Ruiz & Maza 1991) would be consistent with the idea that they are very young galaxies undergoing their first episodes of star formation. On the other hand, in a recent study, Schulte-Ladbeck & Crone (1998) have concluded that in the blue compact dwarf galaxy VII Zw 403 there are older stellar population components.

In a previous study (Raimann et al. 2000, hereafter Paper I) we have investigated the stellar population properties of a sample dominated by nearby H II galaxies, but including also starburst and Seyfert 2 galaxies for comparison purposes. We have considered their continuum and emission/absorption line properties, grouped them into high signal-to-noise templates, and performed stellar population syntheses using a base of stellar cluster spectra (Bica 1988; Bica & Alloin 1986). We concluded that most H II galaxies present important flux contributions from populations as old as 500 Myr.

In the present paper, we investigate the gaseous properties of the templates obtained in Paper I, after subtraction of the

★ E-mail: raimann@if.ufrgs.br (DR); thaisa@if.ufrgs.br (TSB); bica@if.ufrgs.br (EB); jmelnick@eso.org (JM); schmitt@stsci.edu (HS)

Table 1. Average properties of the groups.

Groups	Number of objects	Spectral Type	$\langle M_B \rangle$	$\langle \log L(H\beta) \rangle$ erg s^{-1}	$\langle$Aperture$\rangle$ kpc × kpc	log[W(Hβ] Å	S/N 4200 Å	S/N 5400 Å
G_Cam1148-2020	9	H II	-17.81 ± 1.08	$40.66^{+0.19}_{-0.34}$	1.5×1.8	2.37	16	11
G_UM461	9	H II	-14.99 ± 2.68	$39.27^{+0.19}_{-0.35}$	0.2×0.3	2.33	21	17
G_Tol1924-416	7	H II	-19.96 ± 0.85	$41.61^{+0.32}_{-1.15}$	2.5×3.3	1.98	26	17
G_NGC1487	6	H II	-17.14 ± 1.07	$39.17^{+0.40}_{-0.34}$	0.2×0.3	1.43	19	15
G_Tol1004-296	17	H II	-17.21 ± 1.17	$39.92^{+0.31}_{-1.38}$	0.4×0.6	2.03	38	29
G_UM448	1	H II	-19.46	41.16	1.8×2.1	1.84	21	18
G_Tol0440-381	18	H II	-18.63 ± 0.67	$40.92^{+0.38}_{-0.44}$	1.5×2.7	1.68	21	12
G_UM504	15	H II	-15.86 ± 0.70	$39.32^{+0.22}_{-0.44}$	0.4×0.8	1.39	23	17
G_UM71	36	H II	-17.68 ± 1.19	$40.17^{+0.26}_{-0.71}$	1.1×2.1	1.45	23	16
G_NGC1510	1	H II	-16.93	39.07	0.3×0.4	1.19	26	26
G_Cam0949-2126	9	H II/starburst	-19.73 ± 1.48	$41.11^{+0.26}_{-0.68}$	2.5×3.8	1.47	21	13
G_Mrk711	5	H II/starburst	-19.81 ± 0.81	$41.22^{+0.21}_{-0.48}$	1.4×2.1	1.47	40	26
G_UM140	15	H II/starburst	-18.09 ± 0.85	$39.73^{+0.17}_{-0.28}$	0.8×1.5	1.07	19	14
G_NGC3089	11	H II/starburst	-19.29 ± 1.02	$40.51^{+0.23}_{-0.54}$	1.1×2.1	1.21	22	16
G_Mrk710	2	starburst	-18.47	$39.57^{+0.32}_{-1.27}$	0.2×0.4	1.62	20	19
G_UM477	8	starburst	-20.11 ± 0.94	$40.22^{+0.34}_{-0.77}$	0.7×1.4	1.10	24	26
G_UM103	3	Seyfert 2	-19.72 ± 0.39	$40.46^{+0.25}_{-0.58}$	1.8×3.7	1.18	13	11
G_NGC4507	7	Seyfert 2	-19.77 ± 0.79	$40.95^{+0.18}_{-0.31}$	1.7×3.5	1.42	15	19
G_NGC3281	6	Seyfert 2	-19.70 ± 0.96	$40.06^{+0.30}$	1.2×2.4	0.88	13	18

underlying stellar population. We use the emission-line fluxes to classify the spectra according to their excitation characteristics in diagnostic diagrams, to calculate the gaseous abundance and to obtain the age of the last generation of (ionizing) stars. The role of the underlying stellar population, including its effect on the interpretation of data from distant star-forming galaxies and its relation to the emission line properties, is also explored.

We present the data set in Section 2. The diagnostic diagrams are discussed in Section 3. The gas metallicity, the age of the ionizing stellar population and relation between the metallicity and the non-ionizing stellar population are studied in Section 4. Possible uses of emission-line galaxies for cosmological studies are discussed in Section 5. The concluding remarks are given in Section 6.

2 THE SAMPLE

The original sample consists of 185 emission-line galaxy spectra obtained by Terlevich and collaborators, most of them (156) discussed individually in Terlevich et al. (1991). The average aperture used in the observations corresponds to $\approx 1.1 \times 1.9$ kpc. More details can be found in Paper I, where we have grouped the spectra according to their continuum, absorption and emission-line properties, in order to obtain improved signal-to-noise (S/N) ratio spectra. This strategy was necessary to constrain the stellar population syntheses, mainly for the H II groups. The resulting spectral groups are listed in Table 1 ordered from bluer spectra at the top to redder at the bottom of the table. The groups are named after the member galaxy with the best S/N ratio. The number of the galaxies in each group is shown in column 2. In two cases, G_UM448 and G_NGC1510, there were no other similar spectra, and we have thus considered them as 'groups' of only one galaxy. The spectral type, according to distribution of emission-line spectra of the groups in the Baldwin, Phillips & Terlevich (1981, hereafter BPT) diagnostic diagrams, is given in column 3. In column 4 we list the average absolute magnitudes $\langle M_B \rangle$, obtained using the apparent magnitudes and radial velocities from the NASA/IPAC Extragalactic Data base (NED)[1] (see Paper I), for $H_0 = 75$ km s^{-1} Mpc^{-1}, and in columns 5, 6 and 7 we provide the average Hβ emission-line luminosities, average dimensions at the galaxy corresponding to the angular aperture and average Hβ equivalent width, respectively. In columns 8 and 9 we list the S/N ratios in the continuum of each template for spectral regions around $\lambda\lambda$4200 and 5400 Å.

The spectra of the groups were dereddened according to $E(B-V)_{\rm i}$, the internal reddening affecting the stellar population which was obtained in the synthesis (Paper I). The synthesized stellar population from Paper I was then subtracted from the spectrum of each group. The importance of the subtraction of the underlying stellar population for emission-line measurements has been discussed in detail by Bonatto, Bica & Alloin (1989). The main effect is on Hβ, with consequences on gas internal reddening determination and calculated emission-line ratios involving this line. Three representative spectra are shown in Fig. 1. In the top of each panel we show the population-free spectrum and in the bottom the dereddened spectrum previously to stellar population subtraction together with the corresponding synthesized spectrum used in the subtraction. The emission spectra for the remaining groups were presented in Raimann (1998).

The emission-line fluxes of the population-free spectra were then measured and the corresponding values, relative to Hβ, are shown in Table 2. In the cases of line blending (e.g. Hα + [N II]$\lambda\lambda$6548, 84 and [S II]$\lambda\lambda$6717,31) the profiles were constrained by adjusting Gaussians of the same width. We have then calculated the residual gas reddening assuming a Galactic reddening law (Seaton 1979), case B recombination and an intrinsic ratio Hα/Hβ = 2.9 (Osterbrock 1989). Only two groups, G_NGC1510 and G_NGC3281, presented significant gas reddenings with

[1] The NASA/IPAC Extragalactic Data base (NED) is operated by the Jet Propulsion Laboratory, California Institute of Technology, under contract with the National Aeronautics and Space Administration.

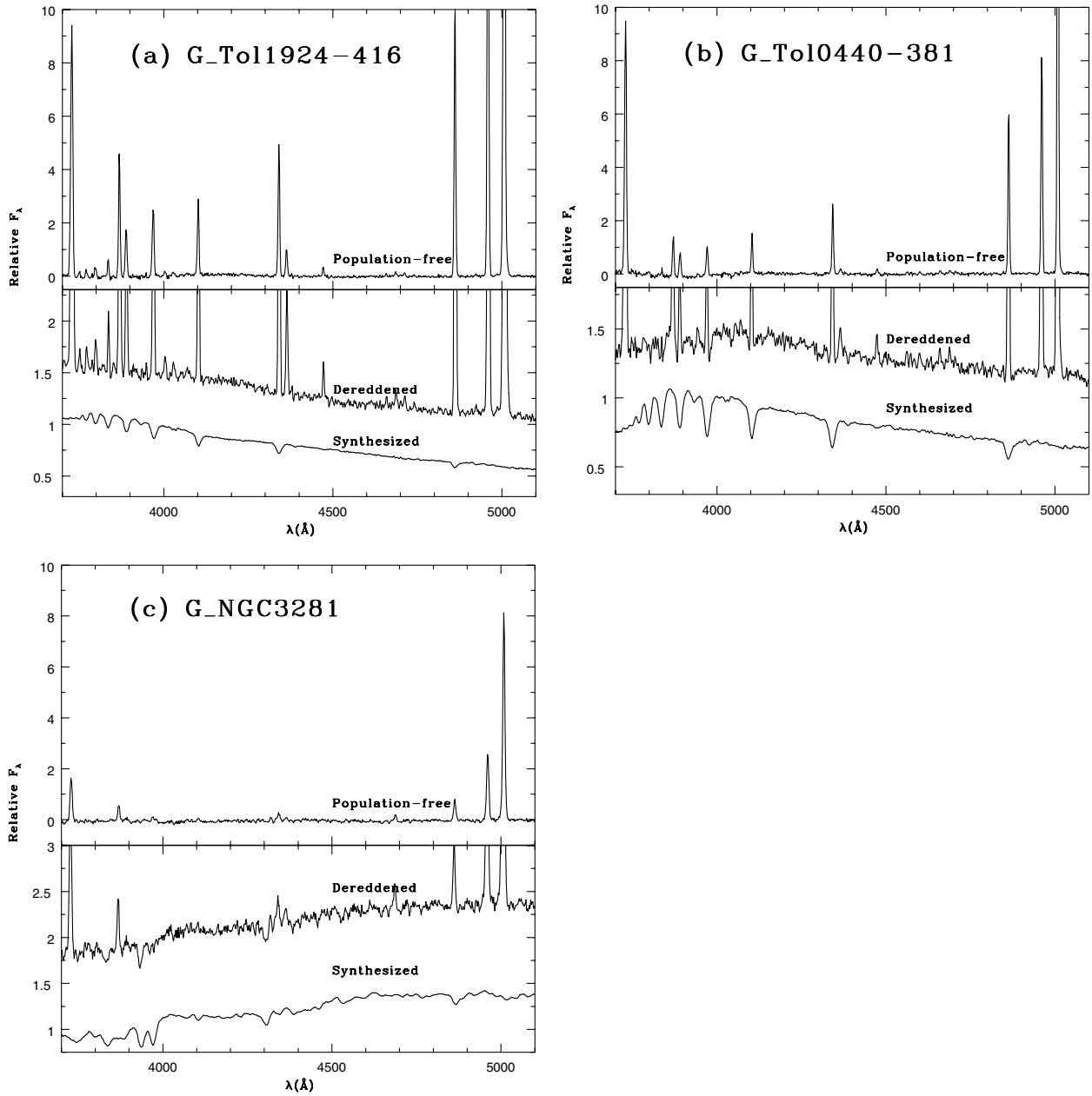

Figure 1. Representative spectral groups: (a) blue H II, (b) H II with Balmer jump in absorption, (c) Seyfert 2. In the bottom panels we present the dereddened spectra and the corresponding synthesized one (Paper I), while in the top panels we present the difference between the two.

$E(B-V)_{\rm gas} = 0.24$ and 0.32, respectively. The other groups have $E(B-V)_{\rm gas} \leqslant 0.05$, which are listed in column 2 of Table 3.

3 BPT DIAGNOSTIC DIAGRAMS

The reddening-corrected emission-line fluxes were used to locate the groups in the BPT diagnostic diagrams log([O III]λ5007/Hβ) versus log([N II]λ6584/Hα), log([O III]λ5007/Hβ) versus log([S II]$\lambda\lambda$6717,6731/Hα) and log([O III]λ5007/Hβ) versus log([O I]λ6300/Hα) (BPT; Veilleux & Osterbrock 1987), shown in Figs 2 and 3.

Fig. 2 contains the present galaxy groups data, together with those of starburst nuclear (therein referred to as MGB), Seyfert, LINER and H II galaxies from Coziol (1996). In this diagram the groups G_UM103, G_NGC4507 and G_NGC3281 are located in the region occupied by Seyfert 2 galaxies while G_UM477 and G_Mrk710 are in the nuclear starburst region. The groups G_Mrk711, G_Cam0949-2126, G_UM140 and G_NGC3089 are located in a region intermediate between those of H II and nuclear starbursts. The remaining groups – the majority – are located in the H II galaxies region. The classification is shown in column 3 of Table 1. It can be observed that the H II galaxy groups are located closer to the H II region loci as defined by the dashed lines in this diagram than the individual H II galaxies of Coziol's (1996) sample.

Fig. 3 contains only our groups data, together with the H II models of McCall et al. (1985). In Fig. 3(a) the H II galaxy groups are also located close to the H II region loci as defined by the dashed line.

Table 2. Emission-line fluxes relative to Hβ.

Group	[O II] λ3727	[Ne III] λ3869	Hγ λ4340	[O III] λ4363	Hβ λ4861	[O III] λ5007	[O I] λ6300	Hα λ6563	[N II] λ6584	[S II] λ6717	[S II] λ6731
G_Cam1148-2020	0.89	0.48	0.50	0.13	1.00	6.25	0.02	2.67	0.04	0.07	0.05
G_UM461	0.86	0.51	0.48	0.12	1.00	6.06	0.01	2.34	0.03	0.05	0.04
G_Tol1924-416	1.15	0.45	0.48	0.10	1.00	5.52	0.02	2.05	0.04	0.07	0.04
G_NGC1487	2.64	0.33	0.48	0.03:	1.00	3.31	$\leqslant$0.01	2.64	0.21	0.24	0.16
G_Tol1004-296	1.53	0.37	0.47	0.05	1.00	4.74	0.03	2.77	0.11	0.12	0.09
G_UM448	2.95	0.22	0.51	0.02	1.00	2.85	0.05	2.69	0.32	0.21	0.17
G_Tol0440-381	1.98	0.26	0.43	0.03	1.00	4.04	0.06	2.44	0.15	0.11	0.10
G_UM504	2.48	0.22	0.34	0.03:	1.00	3.64	$\leqslant$0.01	2.77	0.23	0.29	0.18
G_UM71	2.19	0.24	0.45	0.02:	1.00	3.75	$\leqslant$0.01	2.70	0.22	0.17	0.10
G_NGC1510	1.80	0.19	0.40	0.03:	1.00	3.93	$\leqslant$0.01	3.75	0.39	0.29	0.20
G_Cam0949-2126	2.19	0.09	0.38	$\leqslant$0.01	1.00	1.83	$\leqslant$0.01	2.58	0.42	0.16	0.21
G_Mrk711	2.26	0.14	0.44	$\leqslant$0.01	1.00	2.16	0.09	3.01	0.88	0.30	0.23
G_UM140	2.75	$\leqslant$0.01	0.44	$\leqslant$0.01	1.00	1.35	$\leqslant$0.01	2.87	0.59	0.27	0.34
G_NGC3089	2.03	$\leqslant$0.01	0.37	$\leqslant$0.01	1.00	1.09	$\leqslant$0.01	3.04	0.96	0.38	0.27
G_Mrk710	1.20	$\leqslant$0.01	0.44	$\leqslant$0.01	1.00	0.35	$\leqslant$0.01	3.07	1.12	0.28	0.26
G_UM477	1.05	$\leqslant$0.01	0.43	$\leqslant$0.01	1.00	0.26	$\leqslant$0.01	3.06	1.46	0.35	0.33
G_UM103	2.52	0.63	0.34	0.11	1.00	7.86	0.27	2.55	1.22	$\leqslant$0.01	0.44
G_NGC4507	1.76	0.83	0.49	0.22	1.00	10.2	0.37	2.94	1.75	0.49	0.51
G_NGC3281	2.24	0.68	0.51	0.22:	1.00	10.4	0.41	4.08	4.04	1.00	0.96

Note: The colon symbol indicates a large uncertainty.

Table 3. Analysis results.

Group	$E(B-V)_{\rm gas}$	Ne(cm^{-3})	T^{++}(K)	$(N^+/H^+)^a$	$(S^+/H^+)^a$	$(O/H)^{a,b}$	$(Ne^{++}/H^+)^a$	log(N/O)^b
G_Cam1148-2020	0.00	$\approx$100	15475	5.52	5.10	7.87	7.04	$-$1.44
G_UM461	0.00	$\approx$100	15039	5.29	5.01	7.89	7.11	$-$1.70
G_Tol1924-416	0.00	300	14436	5.56	5.11	7.92	7.10	$-$1.57
G_NGC1487	0.00	$\approx$100	11177	6.51	5.89	8.19	7.32	$-$1.35
G_Tol1004-296	0.00	$\approx$100	11811	6.17	5.57	8.14	7.30	$-$1.39
G_UM448	0.00	258	10294	6.75	5.94	8.32	7.29	$-$1.28
G_Tol0440-381	0.00	330	10475	6.41	5.68	8.31	7.33	$-$1.44
G_UM504	0.00	$\approx$100	10839	6.57	5.97	8.23	7.21	$-$1.29
G_UM71	0.00	151	10082	6.62	5.57	8.32	7.36	$-$1.28
G_NGC1510	0.24	$\approx$100	11011	6.67	5.87	8.21	7.20	$-$1.13
G_Cam0949-2126	0.00	1654	7776	7.15	6.27	8.63	7.45	$-$1.26
G_Mrk711	0.03	141	9109	7.40	6.28	8.58	7.58	$-$0.87
G_UM140	0.00	1354	7727	7.30	6.48	8.65		$-$1.20
G_NGC3089	0.04	$\approx$100	7144	7.56	6.48	8.61		$-$0.86
G_Mrk710	0.05	350	4968	8.00	6.78	8.99		$-$0.81
G_UM477	0.05	330	4611	8.19	6.95	9.05		$-$0.69
G_UM103	0.00	3080	13475			8.69^c		
G_NGC4507	0.01	1048	15797			8.92^c		
G_NGC3281	0.32	755	17285			8.83^c		

^{a} In 12 + log units.
^{b} $12+\log({\rm O/H})_\odot = 8.91$ and $\log({\rm N/O})_\odot = -0.93$.
^{c} Calculated using a different method: the calibration of Storchi-Bergmann et al. (1998; see text).

In order to check if the groups are indeed closer to the theoretical loci than the individual H II galaxies, we have plotted in Fig. 4 the groups data together with the original data for each individual galaxy (Terlevich et al. 1991). It can be observed that the effect is still present. Two factors contribute to this: the subtraction of the stellar population, which increases the Hβ emission (reducing log([O III]/Hβ)), and the grouping of the individual spectra which produces higher S/N spectra. In H II galaxies with significant contribution of $t \geqslant 50$ Myr stellar populations the first effect is particularly important, because these components have strong Balmer absorption lines.

We conclude that with spectra of high S/N ratio and corrected for the stellar population absorptions the H II galaxies in the BPT diagnostic diagrams log([O III]λ5007/Hβ) versus log([N II]λ6584/Hα) and log([O III]λ5007/Hβ) versus log([S II]$\lambda\lambda$6717,6731/Hα) get closer to the theoretical H II region loci presented by Evans & Dopita (1985) and McCall et al. (1985). Previous works have proposed models with very high temperatures to cover the region occupied by H II galaxies (Tresse et al. 1996 and Rola et al. 1997). Our results suggest that this is not necessary and that H II galaxies behave similarly to H II regions. We therefore suggest this observational locus as reference for theoretical models of H II galaxies in the BPT diagrams.

In the diagnostic diagram log([O III]λ5007/Hβ) versus log([O I]λ6300/Hα) (Fig. 3b) the galaxy groups for which it was possible to measure [O I]λ6300 are located close to the H II region loci as defined by the dashed line. However, for many groups – mainly those with the lowest [O III]/Hβ – we have obtained only upper limits for [O I]λ6300; these limits suggest systematically lower values for the galaxies when compared to H II region models. On the other hand, there are not enough H II regions data in the literature with low [O III]/Hβ and with

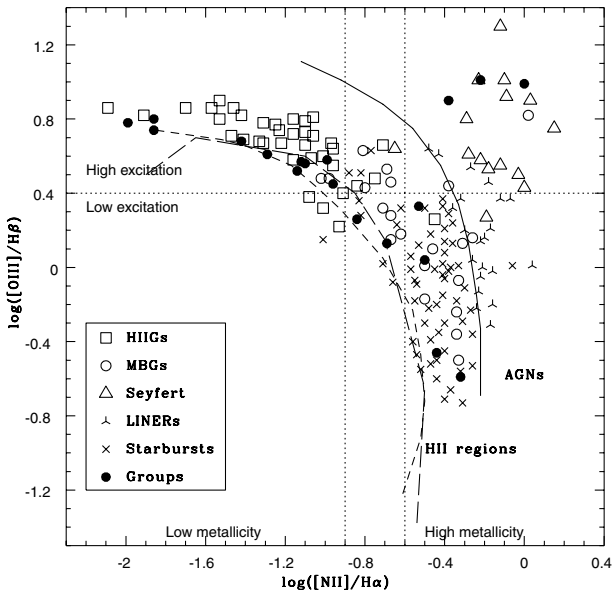

Figure 2. BPT diagnostic diagram log([O III]λ5007/Hβ) versus log([N II]λ6584/Hα), adapted from Coziol (1996) showing the location of the 19 groups (filled circles) as compared to other emission-line galaxies. The continuous line to the right is an empirical borderline separating H II regions from AGNs. The short-dashed curve represents H II region models of Evans & Dopita (1985) and the long-dashed curve, H II region models of McCall et al. (1985).

measured [O I]λ6300, so these models are difficult to be compared even with H II region data.

The only star-forming group which approaches considerably the AGN region is the H II/starburst group G_Mrk711. It would be interesting to study in detail galaxies in this group (Paper I), because they might contain intrinsically high temperature H II regions, or alternatively that locus might reflect a composite spectrum, i.e. AGN mixed to H II region emissions owing to aperture effects (Pastoriza, Donzelli & Bonatto 1999 and Storchi-Bergmann 1991).

4 AGE AND METALLICITY EFFECTS

We now study the gas properties, using the population-free spectra, in order to investigate the gas metallicity and age of the ionizing stellar population, and their relation to the loci occupied by the groups in the BPT diagrams.

4.1 Metallicity

Since the metallicity is very sensitive to gas temperature, which is not uniform in the nebulae, it is important to consider the ionization structure (Garnett 1992). We have adopted the two-zone model of Campbell, Terlevich & Melnick (1986), where the emission-line ratio [O III]$\lambda\lambda$4959, 5007/λ4363 gives the temperature (T^{++}) of the high ionization species (like O^{++} and Ne^{++}) and the emission-line ratio [N II]$\lambda\lambda$6548, 84/λ5755 gives the temperature (T^{+}) of the low ionization species (like O^{+}, N^{+} and S^{+}). The density is obtained through the emission-line ratio [S II]λ6717/λ6731.

We were able to measure [O III]λ4363 for the H II galaxies and Seyfert 2 galaxies, while for the remaining groups only upper limits could be obtained (column 5 of Table 2). For the latter

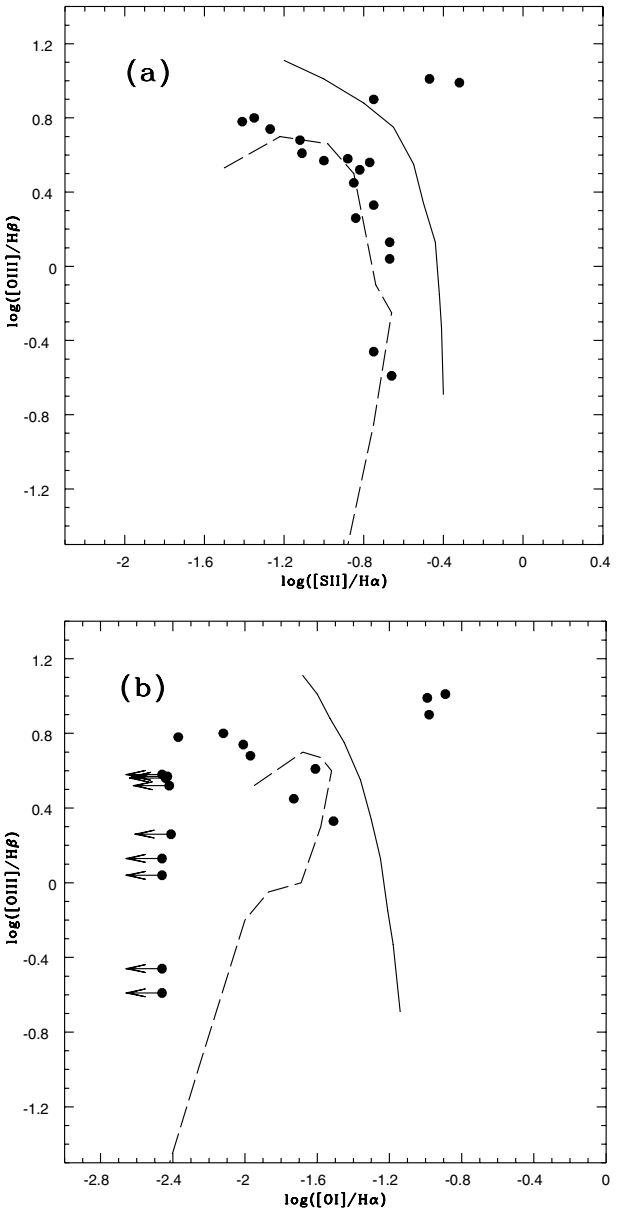

Figure 3. BPT diagnostic diagrams (a) log([O III]λ5007/Hβ) versus log ([S II]$\lambda\lambda$6717,6731/Hα) and (b) log([O III]λ5007/Hβ) versus log([O I] λ6300/Hα). Symbols and curves as in Fig. 2. In diagram (b) arrows indicate upper limits.

groups we have used the empirical calibration of Pagel et al. (1979) extrapolated as described in Schmitt, Storchi-Bergmann & Baldwin (1994) and Storchi-Bergmann, Wilson & Baldwin (1996) to calculate T^{++}. We could not detect [N II]λ5755 in any of the spectra. We have thus used the relation of Campbell et al. (1986) to calculate T^{+}. The ionic abundance calculations were performed using a three-level atom model (McCall 1984).

The resulting T^{++}, Ne and ionic abundances are shown in Table 3. The total oxygen abundance (O/H) was calculated by adding the contributions of O^0, O^+ and O^{++}. The nitrogen abundance was calculated by assuming that $N/O = N^+/O^+$, based upon the rough coincidences between the ionization potentials of the two ions (Storchi-Bergmann, Calzetti & Kinney 1994 and references therein).

The 10 H II galaxy groups (G_NGC1510, G_UM504, G_UM71,

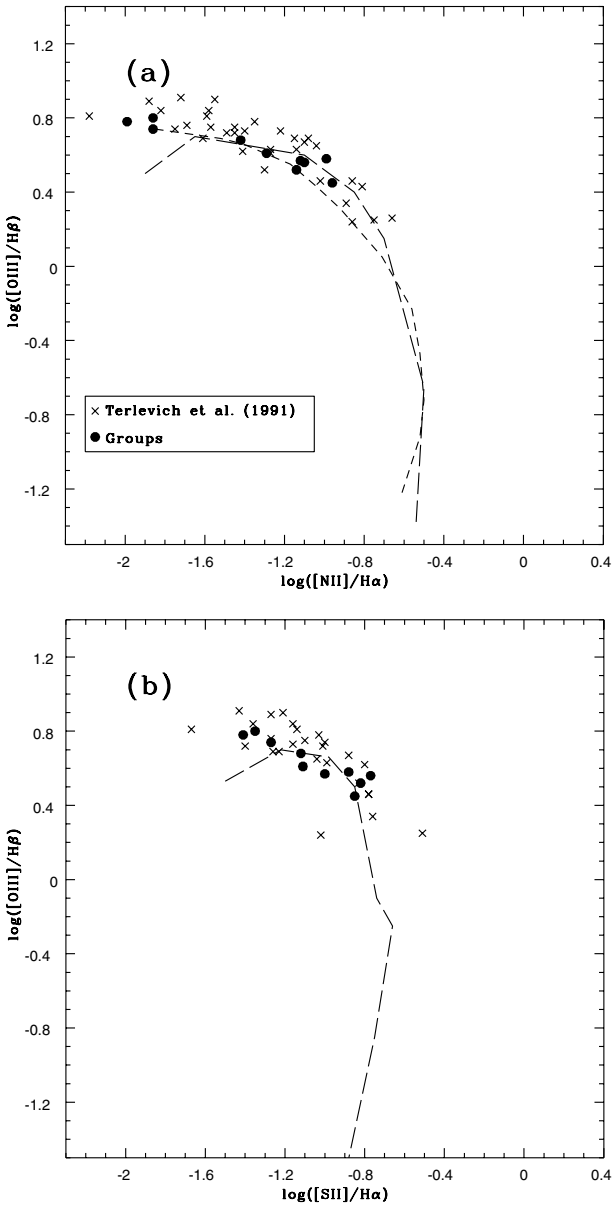

Figure 4. BPT diagnostic diagrams (a) log([O III]λ5007/Hβ) versus log([N II]λ6584/Hα) and (b) log([O III]λ5007/Hβ) versus log([S II] λλ6717,6731/Hα) comparing the groups (filled circles) with the individual galaxies from Terlevich et al. (1991, crosses).

G_UM461, G_Tol1924-416, G_UM448, G_NGC1487, G_Tol1004-296, G_Tol0440-381 and G_Cam1148-2020) span a range in oxygen abundance of $7.87 < 12 + \log(O/H) < 8.32$. With small variations, because of different methodologies and sample, these values agree with those of Peña et al. (1991) and Terlevich et al. (1991). The relatively large metallicities attained by the H II galaxies are consistent with the result found in Paper I, that most H II galaxy groups are not single generation, but present previous generations of stars which have enriched the gas. The groups classified as starbursts – G_UM477 and G_Mrk711 – have near solar metallicity, while the ones classified as intermediate between H II and starburst – G_Cam0949-2126, G_Mrk711, G_UM140 and G_NGC3089 – have somewhat lower metallicity: $12 + \log(O/H) \approx 8.6$.

It can be noticed in Table 3 that the Seyfert 2 groups G_UM103,

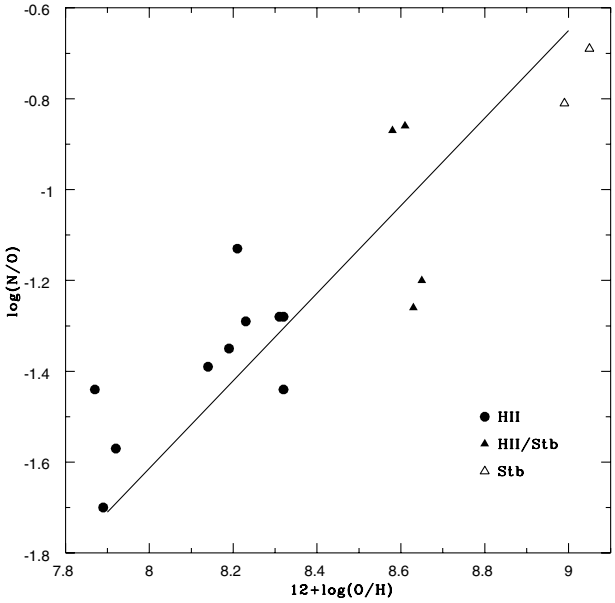

Figure 5. log(N/O) versus 12 + log(O/H) and linear regression of Storchi-Bergmann et al. (1994). Circles represent H II galaxies, open triangles represent starbursts and filled triangles indicate intermediate H II/ starbursts.

G_NGC3281 and G_NGC4507 have very high temperatures when compared with those predicted by photoionization models (Storchi-Bergmann, Bica & Pastoriza 1990), which make the calculated chemical abundances lower than expected. This result is typical of Seyfert galaxies and is owing to density stratification, to the presence of matter-bounded clouds (Binette, Wilson & Storch-Bergmann 1996), collisional de-excitation and a hard ionizing continuum, effects not present in H II regions (Viegas-Aldrovandi & Gruenwald 1988), making the above temperature calibration not valid for the Seyferts. Besides, Storchi-Bergmann et al. (1996) have pointed out how critical is the stellar population subtraction to the measurement of the [O III]λ4363 in Seyfert galaxies, which usually causes one to overestimate the strength of this line.

We have thus revised the metallicities of the Seyfert 2 groups using the calibrations of Storchi-Bergmann et al. (1998) for the narrow-line region (NLR) of active galaxies which do not depend on [O III]λ4363. These calibrations are a function of the emission-line ratios [O III]λλ4959, 5007/Hβ, [N II]λλ6548, 84/Hα and [O II]λ3727/[O III]λλ4959, 5007. We find that the (O/H) abundance is solar for G_NGC4507 and slightly below solar for G_UM103 and G_NGC3281.

In Fig. 5 we show log(N/O) plotted against 12 + log(O/H) for the H II galaxies and starbursts. The distribution of our galaxy groups is consistent with the relation found by Storchi-Bergmann et al. (1994) for star-forming galaxies covering $8.3 < 12 + \log(O/H) < 9.4$ (solid line in this figure). This relation is predicted by a simple model of galactic chemical evolution with instantaneous recycling, in which nitrogen has a secondary origin and oxygen has primary origin (Storchi-Bergmann et al. 1994 and references therein). Vila-Costas & Edmunds (1993) have shown that the secondary behaviour dominates for $12 + \log(O/H) > 8.2$, while for lower abundances nitrogen has mainly a primary origin [log(O/N) is approximately constant]. We have too few galaxies in the low abundance end to reach any conclusion there, but we can say that the data are consistent also with the results of Vila-Costas

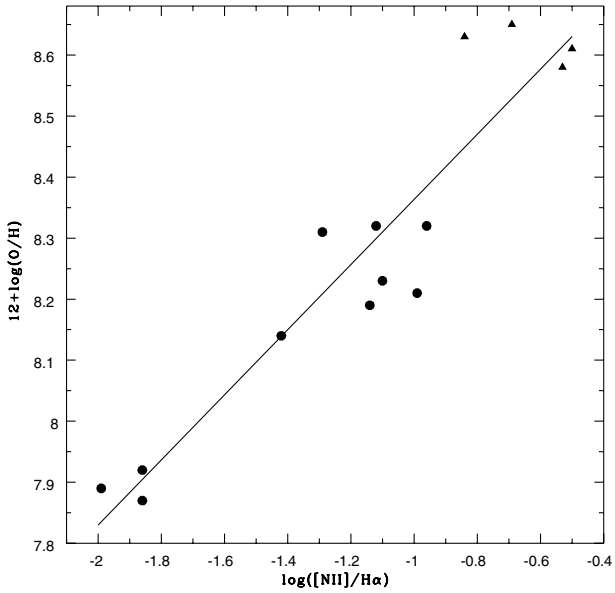

Figure 6. $12 + \log(\mathrm{O/H})$ versus $\log([\mathrm{N\,II}]/\mathrm{H}\alpha)$ and a linear regression to the data. Symbols as in Fig. 5.

and Edmunds, as all data points in the low metallicity end are located above the line denoting secondary behaviour.

Finally, we notice that the BPT sequence of H II galaxies is also a sequence of $[\mathrm{N\,II}]/\mathrm{H}\alpha$ values. We have thus plotted in Fig. 6, $12 + \log(\mathrm{O/H})$ versus $\log([\mathrm{N\,II}]/\mathrm{H}\alpha)$ for the H II and intermediate H II/starburst groups and conclude that they are very well correlated, with a Spearman rank correlation coefficient of 0.90. $\log([\mathrm{N\,II}]/\mathrm{H}\alpha)$ can thus be used as a metallicity index for these galaxies. A linear regression to the data in Fig. 6 gives

$$12 + \log(\mathrm{O/H}) = 8.89(\pm 0.07) + 0.53(\pm 0.06)\log([\mathrm{N\,II}]/\mathrm{H}\alpha).$$

This kind of relation has been found by Storchi-Bergmann et al. (1994) for a sample dominated by more metal-rich starbursts. The main difference encountered here is that, for the lower metallicity H II galaxies of Fig. 6, $[\mathrm{N\,II}]/\mathrm{H}\alpha$ shows a wider dynamical range as a function of $12 + \log(\mathrm{O/H})$ than do the more metal-rich starbursts.

4.2 Age indicators

The equivalent width $W(\mathrm{H}\beta)$, the $[\mathrm{O\,III}]\lambda\lambda 4959, 5007/\mathrm{H}\beta$ ratio and relative volume R of the He^+ and H^+ zones are age indicators for H II regions (Dottori 1981, 1987). Dottori & Bica (1981) have shown that $W(\mathrm{H}\beta)$ can be used to date H II regions of the Magellanic Clouds. Copetti, Pastoriza & Dottori (1986) studied the evolution of the above properties with age through stellar evolution models with a single burst of star formation, which can be used to derive the age of the ionizing star clusters from $W(\mathrm{H}\beta)$ or $[\mathrm{O\,III}]/\mathrm{H}\beta$.

More recently, Stasińska & Leitherer (1996) constructed a new grid of models representing an H II region produced by an evolving starburst embedded in a gas cloud of the same metallicity. They concluded that both $W(\mathrm{H}\beta)$ and $W([\mathrm{O\,III}])$ were good age indicators, but not $[\mathrm{O\,III}]/\mathrm{H}\beta$. According to them, the $[\mathrm{O\,III}]/\mathrm{H}\beta$ ratio is a poor chronometer because its time dependence is mild for ages smaller than 5 Myr and its behaviour is affected by the ionization parameter.

We have thus used the models of Stasińska & Leitherer (1996) to derive the age of the ionizing star cluster for the present H II galaxy groups from the measured $W(\mathrm{H}\beta)$ and $W([\mathrm{O\,III}])$. In Figs 7(a) and (b) we present a sequence of models (continuous line) in $W([\mathrm{O\,III}])$ and $W(\mathrm{H}\beta)$ versus age diagrams together with the data from our groups (horizontal lines). The models with the parameters best suited to our data correspond to $Z = 0.25\,\mathrm{Z}_\odot$.

In the above models the continuum is only owing to the nebular and ionizing stellar population. As concluded in Paper I, in the galaxy groups there is additional contribution of older stellar populations to the continuum, so that it is necessary to subtract that contribution before calculating $W(\mathrm{H}\beta)$ and $W([\mathrm{O\,III}])$. In order to illustrate the effect of this additional component in the derived ages, we present in Fig. 7(b) both the data previously to the subtraction as dashed lines, and the corrected data as solid lines.

The age derived from $W(\mathrm{H}\beta)$ is plotted against the age derived from $W([\mathrm{O\,III}])$ in Fig. 7(c). Although the ages derived from $W([\mathrm{O\,III}])$ are in most cases up to $\approx$1 Myr larger than the ones from $W(\mathrm{H}\beta)$, they are well correlated with Spearman rank correlation coefficient of 0.98. Using both diagrams (Figs 7a and b) we derive an age range of 2.7–5.0 Myr for the ionizing populations in the H II galaxy groups. This age range corresponds to the predicted Wolf–Rayet (WR) phase of a young star cluster (Schaerer & Vacca 1998). Indeed, WR features have been detected in our H II galaxy spectra and were discussed in Paper I.

As the age does not vary much among the H II galaxy groups, the sequence defined in the BPT diagram must be dominated by a varying metallicity (Section 4.1).

An age effect is suggested when we investigate the relation between the gas metallicity and the contribution of the stellar population with ages $t > 100$ Myr to the spectra. This can be observed in Fig. 8 where we plot $12 + \log(\mathrm{O/H})$ against the percentage of stellar population with ages >100 Myr. This diagram suggests that most of the gas enrichment has been produced by stellar populations older than 100 Myr. The H II galaxies are the ones with smallest contributions of stars older than 100 Myr and most metal-poor while the Seyfert galaxies have the largest contributions of older populations and are the most metal-rich. There are only two deviant points, corresponding to the starbursts. These cases can be understood as arising from exceptionally high star formation rates in luminous evolved galaxies, spiral or interacting, so that light from stars younger than 100 Myr dominate the observed fluxes of the galaxies.

5 POSSIBLE COSMOLOGICAL USES

Recently, Melnick et al. (2000) have called attention to the possible use of H II galaxies as cosmological probes. In principle (i) emission-line velocity dispersions, (ii) H II galaxy luminosities as candles, and (iii) stellar population/emission-line properties as probes of galaxy evolution would be important tools to explore. In the following we discuss the latter two possibilities.

As can be seen in Table 1 the $\langle \mathrm{M}_B \rangle$ values vary a lot among H II galaxy groups. Although the sources of B magnitudes are heterogeneous we do not expect that broad-band magnitudes be useful as candles, since the contribution from underlying stellar populations of different ages varies considerably, as found in the population syntheses (Paper I). However, $\mathrm{H}\beta$ emission line luminosities appear to be less dispersed both within and among groups. This is especially so, by considering aperture effects among groups (Table 1). In order to further explore this possibility

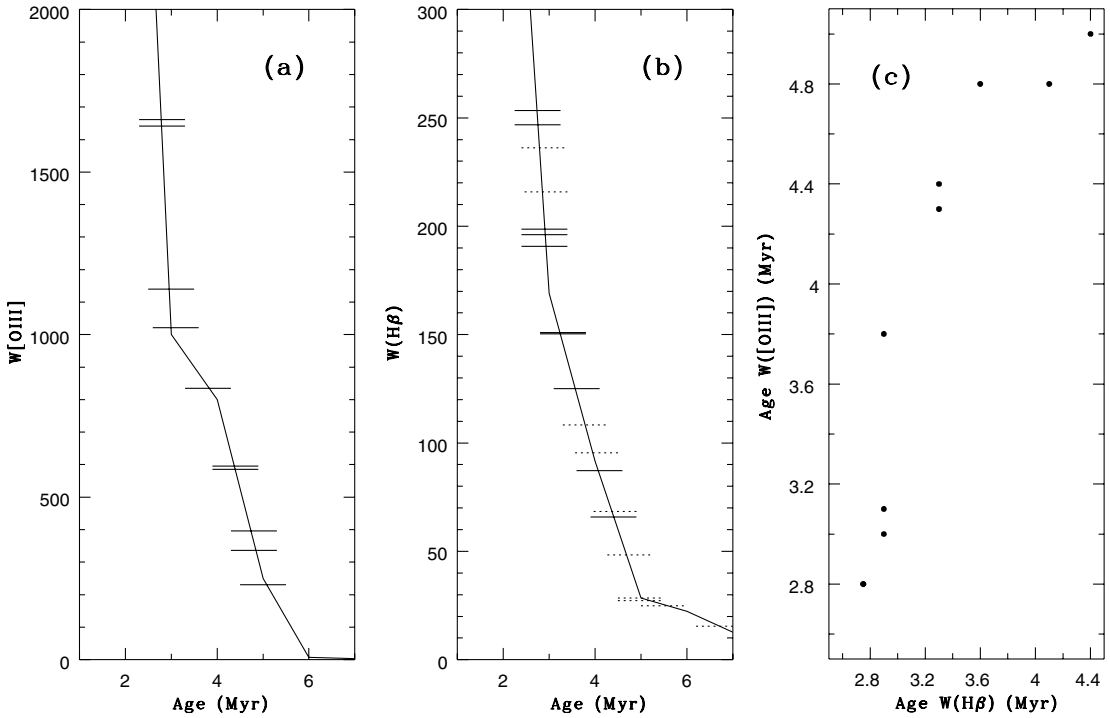

Figure 7. Model sequences (continuous lines) of (a) W([O III]) and (b) W(Hβ) as a function of age of the ionizing stellar population (Stasińska & Leitherer 1996) together with the values of W([O III]) and W(Hβ) for the present sample (horizontal solid lines) used to derive the ages of ionizing stellar population. In (b) we also show the data previously to the stellar population subtraction (horizontal dashed lines). The age derived with W([O III]) is plotted against the age derived with W(Hβ) in (c).

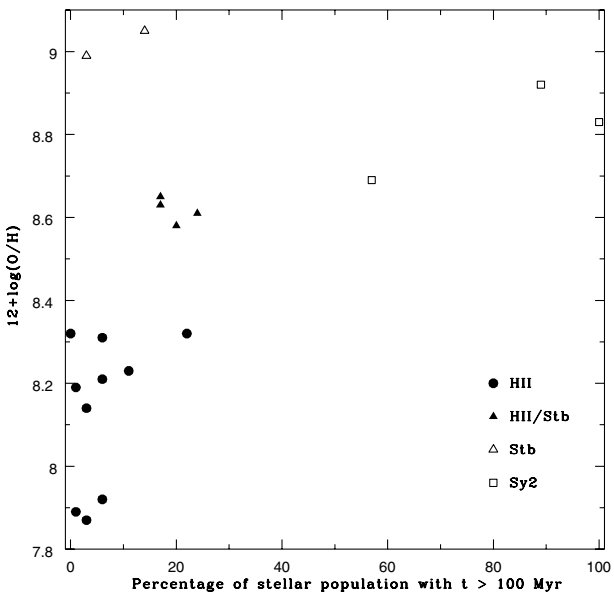

Figure 8. Relation between metallicity and contribution of stellar populations (to the flux at $\lambda = 4020$ Å) older than 100 Myr to the spectrum. Circles represent H II galaxies, squares represent Seyfert galaxies, open triangles represent starbursts and filled triangles indicate intermediate H II/starbursts.

it would be important to observe whole sets of local calibrators by means of narrow-filter CCD imaging in emission lines and neighbouring continuum.

For high-redshift galaxies, many lines used in the traditional diagnostic diagrams move out of the optical spectral range and typically the spectra have a low S/N ratio in the continuum. Frequently, in these cases, the two strongest emission lines observable in the optical window are [O II]λ3727 Å and Hβ. Rola, Terlevich & Terlevich (1997, hereafter R97) used the equivalent widths of these lines to construct new diagnostic diagrams in order to classify the spectra of distant emission-line galaxies observed in deep galaxy redshift surveys.

Our data in the diagnostic diagram W([O II])/W(Hβ) versus log[W(Hβ)] are shown in Fig. 9. In agreement with R97, the Seyfert galaxies occupy the region with $W([\mathrm{O\,II}])/W(\mathrm{H}\beta) \geqslant 3.5$ while the starbursts and H II galaxies occupy the region with $W([\mathrm{O\,II}])/W(\mathrm{H}\beta) \leqslant 3.5$ and $\log[W(\mathrm{H}\beta)] > 1.0$. Although this diagram segregates AGNs from H II/starburst galaxies we find that it does not segregate between H II and starburst galaxies.

We have investigated the effect of the stellar population contribution in the above diagram, by subtracting the contribution of the older age components to the continuum of the H II and starburst galaxies, and leaving only the ionizing continuum for the calculation of the equivalent widths. The result is presented in Fig. 10, which shows a shift in the loci of the galaxies with W(Hβ) as low as $\approx$10 Å to values larger than 50 Å, and for the W([O II])/W(Hβ) from values as large as $\approx$3 down to values lower than 1.5. It can be concluded that equivalent widths W([O II]) and W(Hβ) of starburst and H II galaxies show a much smaller range of values once the older stellar population contributions are subtracted, which means that the intrinsic properties of star-forming regions do not vary as much as suggested by the diagram before subtraction (Fig. 9). In fact, we conclude that the value of log[W(Hβ)] can be used as an indicator of the percentage contribution of the non-ionizing stellar population to the continuum. In Fig. 11 we plot this percentage P against log[W(Hβ)] together with a linear regression

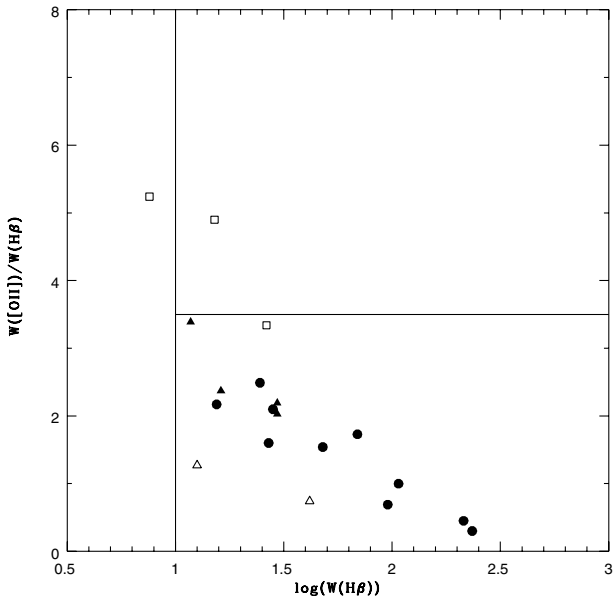

Figure 9. Diagnostic diagram W([O II])/W(Hβ) versus log[W(Hβ)] adapted from R97 with our data without subtracting the contribution of older stellar populations to the continuum. Symbols as in Fig. 8.

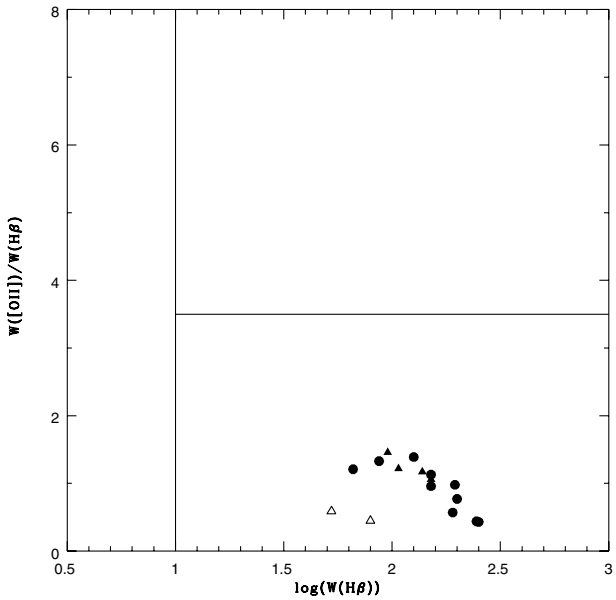

Figure 10. Diagnostic diagram W([O II])/W(Hβ) versus log[W(Hβ)] adapted from R97 with our data after subtracting the contribution of older stellar populations to the continuum. Symbols as in Fig. 8.

to the data

$$P(\%) = 153.04(\pm 8.76) - 56.52(\pm 5.31)\log[W(\mathrm{H}\beta)]$$

for W(Hβ) in Å.

The Spearman rank correlation coefficient to this correlation is −0.90. W(Hβ) is thus a powerful tool for estimating the contribution of older stars to the spectrum of a galaxy. The relation above is very useful, especially for distant galaxies, for which W(Hβ) can be obtained once a continuum can be detected underneath Hβ.

On the other hand, back to the R97 diagram, we can conclude

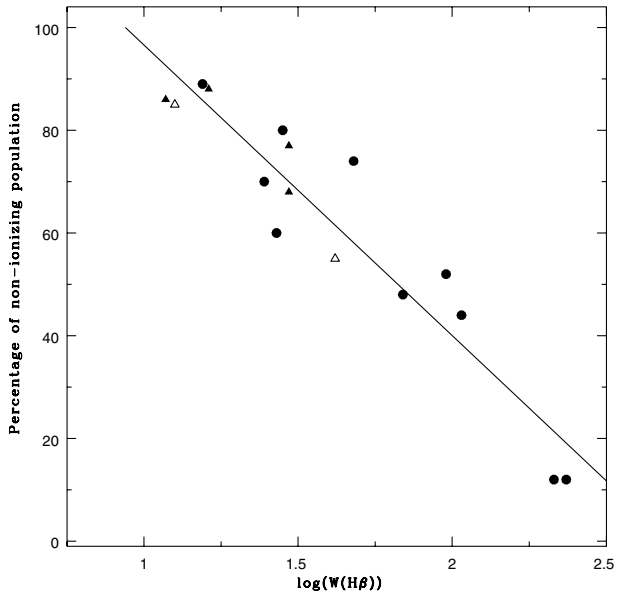

Figure 11. Relation between percentage of non-ionizing stellar population to the flux at $\lambda = 4020$ Å and log[W(Hβ)]. The straight line is a linear regression to the data. Symbols as in Fig. 8.

that the correction by the stellar population does not move the H II and starburst galaxies to regions in the diagram outside the limits suggested by R97. However, for very distant galaxies, age ranges will necessarily become narrower and fractions of intrinsically young galaxies should increase; in both cases the lower right part of R97's diagram should become more and more populated for such high-redshift samples, as simulated in our analysis above.

6 CONCLUDING REMARKS

We have analysed the emission-line spectra of 19 galaxy templates, obtained from the grouping of 185 emission-line galaxy spectra, as described in Paper I. After correction for internal reddening and subtraction of the synthesized population spectrum, both from Paper I, the emission-line fluxes of each template were measured and corrected for additional gaseous reddening, when present. According to the corresponding locus of each template in the BPT diagrams, the present sample comprises 10 groups of H II galaxies, three groups of Seyfert 2 galaxies, two groups of nuclear starbursts and four groups of intermediate cases between nuclear starbursts and H II galaxies.

The H II galaxy groups define a much tighter sequence in the BPT diagrams than the individual galaxies, suggesting that the spread obtained in previous studies is owing to a combination of lower S/N ratio spectra and of not taking into account the contribution of the underlying stellar population. With population subtraction in spectra of improved S/N ratio, the H II galaxy groups get closer to the theoretical sequences of H II regions presented by Evans & Dopita (1985) and McCall et al. (1985), suggesting that they are more similar to H II regions than concluded in previous works. The resulting sequence of H II templates in the BPT diagram is suggested as a fiducial observational locus for future models of H II galaxies.

From the emission-line ratios, we calculate the gas metallicity and age of the ionizing stellar population, and investigate the effect of these two parameters in the BPT diagram above. We conclude that the sequence defined by the H II galaxy templates is

primarily owing to metallicity, which spans the range $7.87 < 12 + \log(\mathrm{O/H}) < 8.32$ ($\approx 1/11$ to 1/4 solar), while the age of the ionizing stellar population ranges only from 2.7 to 5.0 Myr.

A connection with age is suggested when we relate the gas metallicity with the percentage contribution of stellar population components older than 100 Myr, which may indicate that the metal enrichment is mostly owing to previous stellar generations, whose signatures are present in the spectral distribution even for the bluest H II galaxies, as discussed in Paper I. The larger the contribution of older stellar components, the more metal rich is the gas. We find a good correlation between $\log([\mathrm{N\,II}]/\mathrm{H}\alpha)$ and $12 + \log(\mathrm{O/H})$ and propose a calibration to obtain the latter from the former.

We also explore the effect of the stellar population contribution to the equivalent width diagnostic diagrams of R97. We conclude that the observed ranges in $W([\mathrm{O\,II}])/W(\mathrm{H}\beta)$ and $W(\mathrm{H}\beta)$ are essentially owing to the non-ionizing stellar population contribution. By relating $\log[W(\mathrm{H}\beta)]$ to the percentage contribution of this population, we conclude that there is a tight correlation between these two quantities. We thus propose a calibration that can be used to estimate the non-ionizing stellar population contribution to the spectra from the measured $W(\mathrm{H}\beta)$, which is particularly useful for probing properties of distant galaxies.

ACKNOWLEDGMENTS

TSB, EB and HS (during part of this work) acknowledge support from the Brazilian Institution CNPq, and DR from CAPES. We thank Iranderly F. de Fernandes (as CNPq undergraduate fellow) for work related to this project. We thank an anonymous referee for valuable suggestions which helped to improve the paper.

REFERENCES

Baldwin J. A., Phillips M. M., Terlevich R., 1981, PASP, 93, 5 (BPT)
Bica E., 1988, A&A, 195, 76
Bica E., Alloin D., 1986, A&AS, 66, 171
Binette L., Wilson A. S., Storchi-Bergmann T., 1996, A&A, 312, 365
Bonatto C., Bica E., Alloin D., 1989, A&A, 226, 23
Campbell A., Terlevich R., Melnick J., 1986, MNRAS, 223, 811
Copetti M. V. F., Pastoriza M. G., Dottori H. A., 1986, A&A, 156, 111
Coziol R., 1996, A&A, 309, 345
Dottori H. A., 1981, A&SS, 80, 267
Dottori H. A., 1987, Rev. Mex. Astron. Astrofis., 14, 463
Dottori H. A., Bica E., 1981, A&A, 102, 245
Evans I. N., Dopita M. A., 1985, ApJS, 58, 125
Garnett D. R., 1992, AJ, 103, 1330
McCall M. L., 1984, MNRAS, 208, 253
McCall M. L., Rybski P. M., Shields G. A., 1985, ApJS, 57, 1
Melnick J., Terlevich R., Terlevich E., 1999, MNRAS, 311, 629
Meurer G. R., Heckman T. M., Calzetti D., 1999, ApJ, 521, 64
Osterbrock D. E., 1989, Astrophysics of Gaseous Nebulae and Active Galactic Nuclei. University Science Books, Mill Valley, CA, p. 80
Pagel B. E. J., Edmunds M. G., Blackwell D. E., Chun M. S., Smith G., 1979, MNRAS, 189, 95
Pastoriza M. G., Donzelli C. J., Bonatto C., 1999, A&A, 347, 55
Peña M., Ruiz M. T., Maza J., 1991, A&A, 251, 417
Raimann D., 1998, MSc thesis, Universidade Federal do Rio Grande do Sul, Brazil
Raimann D., Bica E., Storchi-Bergmann T., Melnick J., Schmitt H., 2000, MNRAS, 314, 295 (Paper I)
Rola C. S., Terlevich E., Terlevich R. J., 1997, MNRAS, 289, 417 (R97)
Schaerer D., Vacca W. D., 1998, ApJ, 497, 618
Schmitt H. R., Storchi-Bergmann T., Baldwin J. A., 1994, ApJ, 423, 237
Schulte-Ladbeck R. E., Crone M. M., 1998, ApJ, 493, L23
Seaton M. J., 1979, MNRAS, 187, 73P
Stasińska G., Leitherer C., 1996, ApJS, 107, 661
Storchi-Bergmann T., 1991, MNRAS, 249, 404
Storchi-Bergmann T., Schmitt H., Calzetti D., Kinney A., 1998, AJ, 115, 909
Storchi-Bergmann T., Wilson A. S., Baldwin J. A., 1996, ApJ, 252
Storchi-Bergmann T., Calzetti D., Kinney A. L., 1994, ApJ, 429, 572
Storchi-Bergmann T., Bica E., Pastoriza M. G., 1990, MNRAS, 245, 749
Terlevich R., Melnick J., Masegosa J., Moles M., Copetti M. V. F., 1991, A&AS, 91, 285
Tresse L., Rola C., Hammer F., Stasińska G., Le Fèvre O., Lilly S. J., Crampton D., 1996, MNRAS, 281, 847
Veilleux S., Osterbrock D. E., 1987, ApJS, 63, 295
Viegas-Aldrovandi S. M., Gruenwald R. B., 1988, ApJ, 324, 683
Vila-Costas M. B., Edmunds M. G., 1993, MNRAS, 265, 199

This paper has been typeset from a TEX/LATEX file prepared by the author.